

Molecular dynamics simulation of the flow mechanism of shear-thinning fluids in a microchannel

Gang Yang(杨刚), Ting Zheng(郑庭), Qihao Cheng(程启昊), and Huichen Zhang(张会臣)
Citation: Chin. Phys. B, 2024, 33 (**4**): 044701. DOI: 10.1088/1674-1056/ad08a7
Journal homepage: http://cpb.iphy.ac.cn; http://iopscience.iop.org/cpb

What follows is a list of articles you may be interested in

Molecular dynamics simulations on the wet/dry self-latching and electric fields triggered wet/dry transitions between nanosheets: A non-volatile memory nanostructure

Jianzhuo Zhu(朱键卓), Xinyu Zhang(张鑫宇), Xingyuan Li(李兴元), and Qiuming Peng(彭秋明)
Chin. Phys. B, 2022, 31 (**2**): 024703. DOI: 10.1088/1674-1056/ac3811

A study of cavitation nucleation in pure water using molecular dynamics simulation

Hua Xie(谢华), Yuequn Xu(徐跃群), and Cheng Zhong(钟成)
Chin. Phys. B, 2022, 31 (**11**): 114701. DOI: 10.1088/1674-1056/ac588a

Energy stored in nanoscale water capillary bridges formed between chemically heterogeneous surfaces with circular patches

Bin-Ze Tang(唐宾泽), Xue-Jia Yu(余雪佳), Sergey V. Buldyrev, Nicolas Giovambattista§, and Li-Mei Xu(徐莉梅)¶
Chin. Phys. B, 2020, 29 (**11**): 114703. DOI: 10.1088/1674-1056/abb664

Numerical simulations of dense granular flow in a two-dimensional channel:The role of exit position

Tingwei Wang(王廷伟), Xin Li(李鑫), Qianqian Wu(武倩倩), Tengfei Jiao(矫滕菲), Xingyi Liu(刘行易), Min Sun(孙敏), Fenglan Hu(胡凤兰), Decai Huang(黄德财)
Chin. Phys. B, 2018, 27 (**12**): 124704. DOI: 10.1088/1674-1056/27/12/124704

Theoretical studies and molecular dynamics simulations on ion transport properties in nanochannels and nanopores

Ke Xiao(肖克), Dian-Jie Li(李典杰), Chen-Xu Wu(吴晨旭)
Chin. Phys. B, 2018, 27 (**2**): 024702. DOI: 10.1088/1674-1056/27/2/024702

Molecular dynamics simulation of the flow mechanism of shear-thinning fluids in a microchannel

Gang Yang(杨刚), Ting Zheng(郑庭), Qihao Cheng(程启昊), and Huichen Zhang(张会臣)†

Naval Architecture and Ocean Engineering College, Dalian Maritime University, Dalian 116026, *China*

(Received 28 August 2023; revised manuscript received 20 October 2023; accepted manuscript online 2 November 2023)

Shear-thinning fluids have been widely used in microfluidic systems, but their internal flow mechanism is still unclear. Therefore, in this paper, molecular dynamics simulations are used to study the laminar flow of shear-thinning fluid in a microchannel. We validated the feasibility of our simulation method by evaluating the mean square displacement and Reynolds number of the solution layers. The results show that the change rule of the fluid system's velocity profile and interaction energy can reflect the shear-thinning characteristics of the fluids. The velocity profile resembles a top-hat shape, intensifying as the fluid's power law index decreases. The interaction energy between the wall and the fluid decreases gradually with increasing velocity, and a high concentration of non-Newtonian fluid reaches a plateau sooner. Moreover, the velocity profile of the fluid is related to the molecule number density distribution and their values are inversely proportional. By analyzing the radial distribution function, we found that the hydrogen bonds between solute and water molecules weaken with the increase in velocity. This observation offers an explanation for the shear-thinning phenomenon of the non-Newtonian flow from a micro perspective.

Keywords: molecular dynamics simulation, non-Newtonian fluid, microchannel, shear-thinning

PACS: 47.50.–d, 52.65.Yy, 83.60.Rs, 82.30.Rs **DOI:** 10.1088/1674-1056/ad08a7

1. Introduction

Non-Newtonian fluids with shear-thinning properties are widely used in microfluidic systems and their rheological properties have a crucial influence on the realization of specific functions.[1–4] Microfluidic systems are often used in biosensors[5] and controllable drug delivery systems.[6] At the same time, owing to the laminarity of the flow in microfluidic systems, they are also broadly used in the precise manipulation of biomass[7] and the separation of particles and cells.[8] The fluids used in most of the above applications are shear-thinning fluids. In a microchannel, the rheological characteristics of the non-Newtonian fluids significantly affect the fluid behavior due to the size effect, making it interesting to analyze the dynamics of shear-thinning fluid flow.[9]

Experimental research has characterized and predicted the characteristics of non-Newtonian fluids in microchannels by summarizing empirical correlations and drawing qualitative conclusions. For example, Mansour *et al.*[10] experimentally investigated the flow of a non-Newtonian fluid (polyacrylamide solution) in a horizontal rectangular microchannel. They pointed out that the pressure drop of the polyacrylamide solution in the microchannel is affected by the rheological flow index and they gave a correlation to predict the pressure drop based on the Lockhart–Martinelli method. Ansari *et al.*[11] measured the velocity profiles of a shear-thinning fluid in a microchannel using particle image velocimetry. The results indicated that the non-Newtonian behavior of the shear-thinning fluid intensified at lower Reynolds numbers and it behaved more like a Newtonian fluid as the Reynolds number increased. At the same time, the velocity profile of non-Newtonian fluids is closer to a top-hat shape than that of Newtonian fluids.

With the development of numerical simulation techniques, the rheological properties of non-Newtonian fluids have been studied through the methods of computational fluid dynamics (CFD). This type of method can better reveal the information of the flow field and draw conclusions that experiments cannot obtain. Miansari *et al.*[12] studied the flow characteristics of the carboxymethyl cellulose solution in a microchannel by performing a computational simulation based on a CFD tool and a finite volume method. Based on the flow-field information, they explained the influence of channel height and Reynolds number on the temperature distribution behavior and pressure drop. Wu *et al.*[13] used the improved lattice Boltzmann method to simulate the non-Newtonian properties of power-law, Bingham and Herschel–Bulkley fluids. They provided expressions of their rheological properties and verified the feasibility of the improved method with the Poiseuille flow law. The results show that the rheological properties of non-Newtonian fluids are affected by the initial yield stress and the flow index.

Molecular dynamics (MD) simulation can reveal the flow mechanism of fluids at the microscopic level and explain the causes of various experimental and CFD results from the perspective of molecules and atoms. Lemarchand *et al.*[14] investigated the rheology and molecular structure of a bi-

†Corresponding author. E-mail: hczhang@dlmu.edu.cn

© 2024 Chinese Physical Society and IOP Publishing Ltd

tumen model with shear-thinning characteristics using non-equilibrium MD simulations. The results showed that the shear-thinning behavior is related to the intermolecular and intramolecular alignments of the solvent molecules and the decrease of the average size of the nano aggregates at high shear rates. Chen *et al*.[15] used MD methods to study the relationship between microstructural evolution and viscosity in a shear-thickening fluid. It was shown that a two-atom structure is formed under a low shear rate because of the strong particle attractions in adjacent layers. When the shear rate is high, the synergetic pair structure extends to a layered structure along the flow direction, leading to a viscosity variation. Bidault *et al*.[16] studied the non-Newtonian properties of silica fibers at high temperatures. The results of the MD simulation showed that the anisotropic structural rearrangement during the drawing process induces a non-Newtonian behavior of the silica fibers with strain-rate-dependent properties. Blanco-Díaz *et al*.[17] performed non-equilibrium MD simulations on the shear flow of an ionic liquid with shear-thinning characteristics. They found that hydrogen bonds play an essential role in the viscosity of the ionic liquid and a decrease in hydrogen bonds results in a decrease in viscosity. In our previous study, we conducted confined shear simulations on systems consisting of sodium carboxymethyl cellulose (CMC) and water molecules to deepen the understanding of the shear-thinning properties of non-Newtonian solutions.[18] According to the results of radial distribution function (RDF) and layer velocity, the weakening of the hydrogen bonding between solute molecules and water is the main reason for the shear-thinning characteristics of CMC solutions.

In general, most research on the flow characteristics of non-Newtonian fluids in microchannels is limited to experiments and CFD. At the same time, there are few explanations for the flow characteristics in microchannels from a micro perspective. Hence, to deepen the understanding of flow behavior in microchannels, the flow of shear-thinning fluid was simulated by using an MD method in this study. The shear-thinning characteristics of non-Newtonian fluids are reflected in the calculation results of the velocity profile and the interaction energy between the walls and the fluid. We also found that the distribution of the velocity profile is related to the number density of particles in the fluid. Meanwhile, the shear-thinning characteristics of non-Newtonian fluids can be explained by the changes in the strength of the hydrogen bonds in the solution.

2. Simulation and method

The flow behaviors of solution systems comprising water and sodium CMC molecules in certain proportions in a 2 nm wide microchannel are investigated. CMC molecules are formed by the polymerization of similar monomers and the molecular formula is $[C_6H_7O_2(OH)_2OCH_2COONa]_m$. In practice, the degree of polymerization of CMC (m) molecules exceeds 200 and their molecular weight can reach up to millions. Constructing molecules with such a large degree of polymerization requires significant computational resources. Most shear-thinning fluids are composed of substantial chain-like molecules and the molecular weight of such high-molecular solutes can reach thousands or even millions. When the solution is subjected to shear, these relatively scattered and tangled chain molecules are affected by the shear stress between the flow layers, which reduces the mutual hooking and rolling rotation and causes them to shrink into agglomerates, showing shear-thinning characteristics.[19,20] The present study focuses on exploring the impact of the interaction between CMC and water molecules on the non-Newtonian properties of the solution. It can be seen from the simulation results in Section 3 that the CMC solution simulated using a monomer can exhibit non-Newtonian characteristics. Meanwhile, using CMC molecules with a polymerization degree of 1 is sufficient to study the interaction between the functional groups of solute and water molecules while saving computing resources, which is significant for guiding subsequent research on long chains. Based on our previous study,[18] density stability analysis was performed for molecular systems with different polymerization degrees. The results show that when m is 1, the density is still reasonable and the CMC monomer ($m = 1$) is selected as the solute molecule of the fluid.

The COMPASS forcefield is used in the simulation, which provides the functional relationship between energy and distance among atoms. It has a broad coverage of covalent molecules, including most common organics, small inorganic molecules and polymers.[21] The results of the current simulations are based on the atomic coordinate information.

The Lennard–Jones 9–6 function was employed to describe the van der Waals interaction. The van der Waals interaction potential (V) is expressed as

$$V(R) = 4\varepsilon\left[\left(\frac{\sigma}{R}\right)^9 - \left(\frac{\sigma}{R}\right)^6\right], \tag{1}$$

where R is the distance between particles, ε is the value of the potential function at the minimum point when $R = 2^{1/6}\sigma$ and σ is the value R at the zero of the potential function.

The Coulomb function was employed to describe the electrostatic interaction and the Coulomb potential (U) is calculated as

$$U(R) = \frac{1}{4\pi\varepsilon_0}\frac{q_i q_j}{R}, \tag{2}$$

where ε_0 is the vacuum permittivity and q_i and q_j represent the residual charge of the two interacting particles.

The Ewald summation method was used in the calculations of van der Waals and electrostatic interactions. This summation method is suitable for periodic and solution systems, with highly accurate calculation results.[22]

2.1. Model setup

Amorphous CMC solutions were created by mixing the CMC and water molecules and packing them into a rectangular cell using the forcefield. We ensured that the wall length ($x = 100$ Å) and the flow width ($z = 20$ Å) in the control groups were the same for comparative analysis. To ensure that the molecular numbers in the solution layers were integers, after determining the number of molecules and specifying the value of x and z, we applied a forcefield to the solution layer to build a solution model. The size of the solution layer in the y-direction was determined by the number of molecules and the forcefield. The configuration of the four-solution systems is shown in Fig. 1(a). Table 1 shows the parameters of the four solution layers.

Table 1. Parameters of the solution layers.

Names of model	Number of CMC molecules	Number of water molecules	Layer size $X \times Y \times Z$ (Å^3)
Water	0	4374	$100 \times 65 \times 20$
9CMC	9	4374	$100 \times 69 \times 20$
18CMC	18	4374	$100 \times 75 \times 20$
27CMC	27	4374	$100 \times 77 \times 20$

Two identical Fe slabs, each with a thickness of 11.5 Å, were used as the microchannel boundary. A sandwiched solution system consisting of two Fe layers and a fluid layer was established to simulate the flow in the microchannel, as shown in Fig. 1(b).

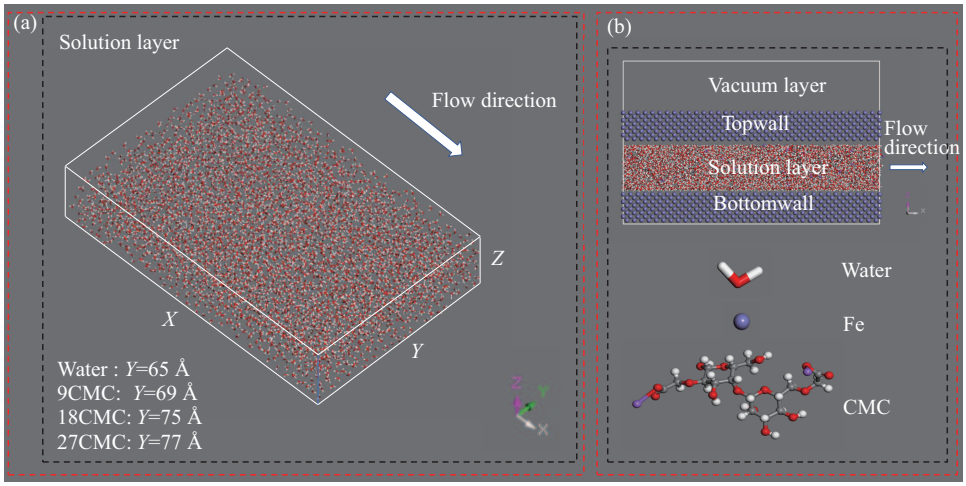


Fig. 1. (a) Solution layers. (b) Simulation system.

2.2. Simulation steps

Optimization of the simulation systems was performed with the following steps: Firstly, the positions of the Fe atoms were fixed to prevent the boundary layer from moving. Then, geometry optimization was performed for preliminary relaxation of the simulation system. The smart algorithm was used for the geometry optimization and the maximum iteration was set to 500 with no external pressure. Secondly, a five-cycle anneal task was utilized for each simulation system with an NVT ensemble from 300 K to 500 K and the total number of dynamics steps was 50000 with a time step of 1 fs. Finally, the trajectory file with the lowest energy was selected from the results of the annealing task as the initial flow state of the flow simulation.

The flow was induced by subjecting the solution layers to external driving fields with the same acceleration. The fluid molecules were moved based on Newton's second law. According to the mass of the solution layers, the corresponding external force is given to the solution layer along the x-direction to acquire the same acceleration. The velocity of the solution layer increases as the external force is applied. This process was carried out in a dynamics task using Forcite, with a calculation lasting 300 ps. The NVT ensemble was used in the dynamics process and the time step was 1 fs.

In order to select the appropriate acceleration to drive the solution layers, we referred to the research of Cao *et al.*[23] and tried three driving fields with different accelerations ($a_1 = 10^{12}$ m/s^2, $a_2 = 10^{13}$ m/s^2 and $a_3 = 10^{14}$ m/s^2) to select the proper one for further simulation. According to the test, the driving force corresponding to a_1 was not enough to overcome the resistance to drive the solution layer. In addition, the solution layer has no apparent parabolic velocity profile, as mentioned in the research of Ansari *et al.*[11] and Abiev.[24] a_3 was too large for the systems and each part of the solution layer reached a considerable speed in a short time, so it was difficult to distinguish the difference between different solutions. Hence, a_2 was the most suitable driving field, which made the solution systems present an evident top-hat-

shaped velocity profile. At this magnitude of acceleration, the solution layer can reach laminar flow conditions with a lower Reynolds number to facilitate further research, as described in Subsection 2.3.

2.3. Feasibility verification

In order to prove the rationality of the acceleration selection and the feasibility of the simulation system, the mean square displacement (MSD) was calculated for the solution layers to determine the motion state of the fluids. The displacement characteristics of molecules in solution can be expressed by

$$\mathrm{MSD} = \left\langle |r(t) - r(0)|^2 \right\rangle, \tag{3}$$

where $r(t)$ is the coordinates of the molecules in the solution, t is the simulation time and $r(0)$ is the initial coordinates of the molecules.

Since the displacement of the solution molecules in the y- and z-directions is small, only the displacement in the x-direction was considered when calculating the MSD. As shown in Fig. 2, after accelerating through the same acceleration field, the average motion states of the four solutions are basically the same and the displacements of the solutions layers are about 1.6 nm. The error of the displacement of the four liquids is less than 1.5%. The result shows that the simulation method of driving the solution layer with the same acceleration (a_2) is feasible, which is helpful to the comparative study of flow characteristics of different solutions.

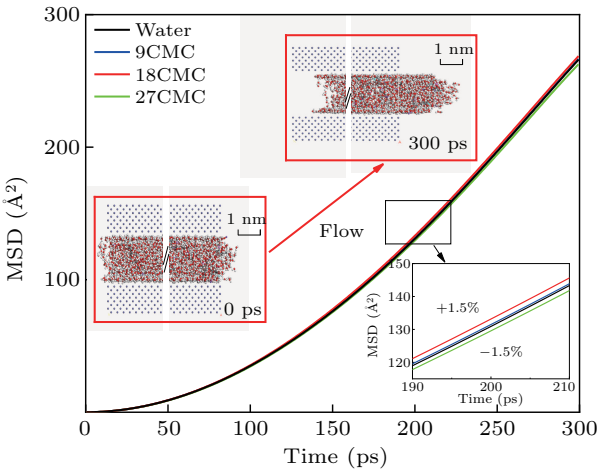


Fig. 2. The MSD of the solution layer.

Meanwhile, we calculated the maximum Reynolds number in the simulation systems according to the parameters of the water

$$Re_{\max} \leq \frac{\rho_{\mathrm{w}} v_{\max} d_{\mathrm{H}}}{\mu_{\mathrm{w}}}, \tag{4}$$

where ρ_{w} is the density of water, μ_{w} is the viscosity of the water, $v_{\max}$ is the maximum velocity that the solution layer can theoretically reach ($v = at$) and d_{H} is the hydraulic diameter.

The Reynolds number of the fluid in this study is less than 10.78, indicating that the flow is laminar. Most of the existing experimental studies on microfluidics are conducted under the condition of a low Reynolds number,[25–27] so the present study is relatively reasonable and also meaningful for practical applications.

3. Result and discussion

Section 3 is organized in the following way: The influences of the non-Newtonian characteristics of the fluids on the velocity profile distribution and fluid–wall interaction energy are shown in Subsections 3.1 and 3.2, respectively. Subsection 3.3 shows the relationship between the velocity profile and the molecule number density distribution in the solution and illustrates the effect of the molecule number density on flow velocity. In Subsection 3.4, the microcosmic reason for the shear-thinning effect in the flow is explained by the change of the specific hydrogen bonding with the flow velocity.

3.1. Velocity profile distribution of the fluid

The velocity profile provides the most fundamental information for understanding the microflow characteristics. Figure 3 shows the velocity profile perpendicular to the direction of flow. The average velocity profile was calculated from 0 ps to 200 ps when the solution layer is accelerated and both the Newtonian and the non-Newtonian fluids have a parabolic velocity profile. These results have been observed in many studies of MD simulations on liquid flows.[23,28,29] The velocity profile shapes of the four solutions are different, which is not inconsistent with the results of the MSD because the MSD calculates an average effect of the entire solution layer. Although the velocity of water is larger at the center of the channel, its velocity near the wall is smaller than that of the CMC solutions. At this time, the overall displacement of both of them is the same.

The velocity profile results are almost symmetric about the central axis of the channel. The layer near the wall is labelled layer 1 (12 Å–15.6 Å) and the next layer is labelled layer 2 (15.6 Å–18.3 Å), as shown in Fig. 3. The stratification approach is derived from the molecule number density results in Subsection 3.3. Figure 3(a) shows the comparison of the velocity profiles of non-Newtonian fluid (18CMC) and Newtonian fluid (water). Newtonian fluids are similar to non-Newtonian fluids in shape and the velocity is minimal near the wall. As the distance from the wall gradually grows, the velocity also gradually increases. This is because the fluid molecules closer to the wall are more attracted by the wall, which makes the fluid suffer more resistance, resulting in a lower velocity. This phenomenon has also been reported by Faraji *et al.*[30] in their Poiseuille flow results for argon atomic fluids through an MD method.

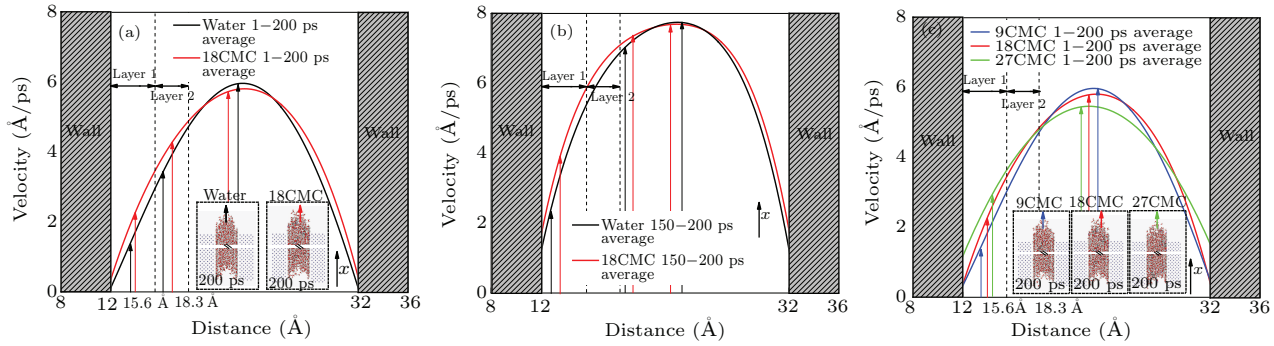


Fig. 3. (a) The velocity profile of the water and 18CMC solution (1–200 ps). (b) The velocity profile of the water and 18CMC solution (150–200 ps). (c) The velocity profile of the CMC solutions with different concentrations (1–200 ps).

The difference between Newtonian fluid and non-Newtonian fluid is that, at layer 1 and layer 2, the velocity of 18CMC is greater than that of water. At layer 1 and layer 2, due to the stronger effect of the wall on the fluid, these positions are subject to more significant shearing. As mentioned in the study of Ansari *et al.*,[11] the deviations of the velocity profile of non-Newtonian fluids from the parabolic shape observed in water are due to the viscosity variations of the non-Newtonian fluids in the different shear rate regions of the flow. The shear effect reduces the viscosity of the non-Newtonian fluid in layer 1 and layer 2, reduces the flow resistance of the fluid, and thus obtains a more extensive velocity than water.

Figure 3(b) shows the velocity profile comparison of water and 18CMC at a higher velocity (150–200 ps). The velocity profile shape of the water and 18CMC is closer to the top-hat shape as the velocity increases. However, the velocity profile of 18CMC is still closer to the top-hat shape than that of water under the same acceleration conditions. It is worth noting that when the velocity is higher, the velocity profile shape of 18CMC is close to that of water, reflecting the shear-thinning characteristics of the CMC solution.

Ansari *et al.*[11] also used the simplified momentum conservation equation to give the expression of the velocity profile of the fluid in a microchannel

$$\frac{u(z)}{u(0,\max)} = 1 - \left(\frac{2z}{d_{\mathrm{H}}}\right)^{\frac{n+1}{n}}, \tag{5}$$

where n is the power law index of the non-Newtonian fluid and u (0, max) is the maximum velocity in the center of the channel.

According to Eq. (5), within the calculation range of the shear-thinning fluid ($0 < n < 1$), the smaller n is, the closer the shape of the velocity profile curve is to the top-hat shape. It can be concluded from Eq. (5) that the velocity profile of non-Newtonian fluid is not only related to the position in the channel but also to the property parameters of the non-Newtonian fluids (the power law index, n).

Figure 3(c) shows the velocity profile of the CMC solutions with different concentrations. It can be seen that the shape of the velocity profiles of the CMC solutions with higher concentrations is closer to the top-hat shape. Higher-concentration CMC solutions have greater velocity at layer 1 and layer 2. A shear-thinning fluid with a higher concentration has a lower n value, contributing to stronger shear-thinning characteristics in the fluid.[31,32] The purpose of introducing Eq. (5) is to verify the trend of our simulation results. The value of n in Eq. (5) cannot be determined in the simulation. As shown in Fig. 4, based on Eq. (5), the normalized velocity profiles are given, which are plotted for different non-Newtonian shear-thinning flows ($n = 0.3$, 0.5 and 0.7). Figure 4 also includes a comparison of Eq. (5) and the present results. We can conclude from Fig. 4 that the smaller the value of n, the closer the shape of the velocity profile is to the top-hat, which is consistent with our simulation results in Fig. 3(c). In conclusion, the velocity profile of a shear-thinning fluid with a lower power law index will be more top-hat-shaped and have greater velocity near the walls.

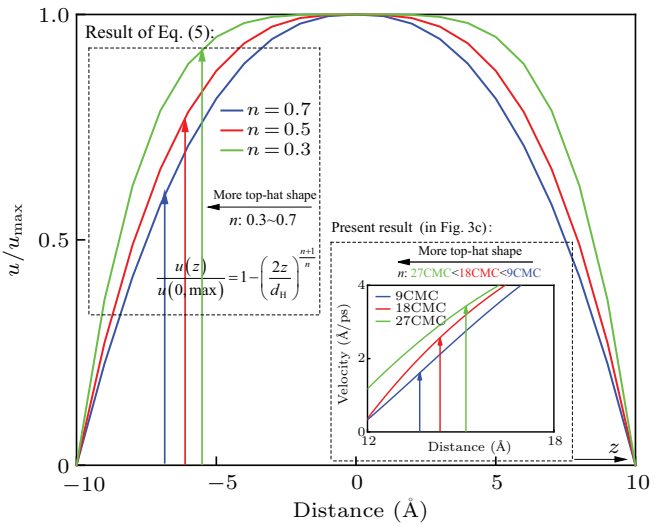


Fig. 4. Normalized velocity profiles of different non-Newtonian flows ($n = 0.3$, 0.5 and 0.7).

3.2. Interaction energy between the wall and the fluid

In order to understand the interaction between the channel walls and the solution layer, the walls and the fluid were considered as two parts, and their interaction energy was cal-

culated. Figure 5 shows the energy structure diagram of the simulation model.

The interaction energy (E_{int}) is calculated by

$$E_{int} = E_{total} - (E_w + E_f), \tag{6}$$

where E_{total} is the total energy of the simulation system, E_w is the energy of the two walls and E_f is the energy of the flow.

All the energy values were calculated by the energy calculation in the Forcite module and the time step was 1 fs. A script was used to calculate E_{int} within 300 ps and obtain the interaction energy function relative to time. As shown in Eq. (6), when calculating E_{total}, the effect of the acceleration field on the energy is considered and the same was done for E_f. Therefore, the (E_{total}–E_f) removes the influence of external forces, according to Eq. (6). So, E_{int} is only related to the motion state of the solution, not to the external force. As shown in Fig. 6, all E_{int} values are negative, indicating that the fluid is attracted by the walls in the microchannel.

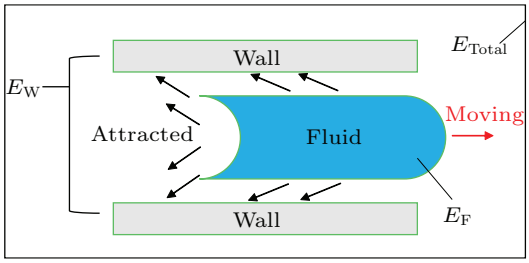


Fig. 5. Energy structure diagram of the simulation model.

Figure 6 also shows that a solution with a higher concentration has a bigger E_{int}. This means that the higher the viscosity, the greater the resistance to motion in the microchannel. Moreover, the interaction energy between the wall and the fluid layer is not only related to the distance but also to the molecular numbers. The more concentrated solution layer has a larger molecular number, which results in a larger interaction energy. When the fluid flows in the microchannel, the effect of the attraction of the wall to the fluid on the flow resistance is not negligible due to the size effect.[33]

In most experiments, the fluid's resistance to motion is reflected by the pressure drop characteristic.[3,9,10] The results obtained in experiments are consistent with the interaction energy simulation results: the higher the concentration of non-Newtonian fluid, the greater the pressure drop and the greater the interaction energy. It can also be seen from Fig. 6 that E_{int} increases somewhat at the beginning of the movement, decreases gradually with the increase of velocity and displacement, and eventually reaches a relatively stable state. This phenomenon is similar to the interaction potential between molecules.

It is noteworthy that the E_{int} of the shear-thinning fluid decreases faster than that of the Newtonian fluid. The interaction energy between the solution layer and the wall will continue to decrease until it fluctuates up and down at a stable value. The time when the mean value of the stable region (250–300 ps) has just been reached is taken as a critical time t, as shown in Fig. 6. The time for the CMC solution to reach a relatively stable state (t_c) is less than that for water (t_w) and the time decreases with the increase of concentration. This indicates that the attraction of the wall to the non-Newtonian fluid decreases rapidly as the velocity increases and the speed of the decrease is greater than that of water. As the flow velocity of a non-Newtonian fluid increases, the interaction energy decreases rapidly due to the decrease in its viscosity. The viscosity of a solution is a macroscopic property. From a microscopic perspective, viscosity is a resistance to movement caused by the mutual attraction and constraints between molecules. The decrease in interaction energy indicates that the attraction and restraint between molecules are no longer tight, and the movement resistance of the solution is reduced. Therefore, the decrease in interaction energy shows a macroscopic viscosity decrease from a microscopic perspective. Moreover, because of the shear-thinning effect, the hydrogen bonding between CMC and water molecules weakens. The constraints on the CMC molecules are reduced and the CMC molecules will be slightly stretched, reducing the resistance, which makes the system more active, causing the interaction energy to drop faster. This reflects the shear-thinning characteristics of the fluid from an energetic point of view. In addition, the interaction energy between the Newtonian fluid and the walls reaches a steady state later because its viscosity does not change and its resistance to motion decreases more slowly.

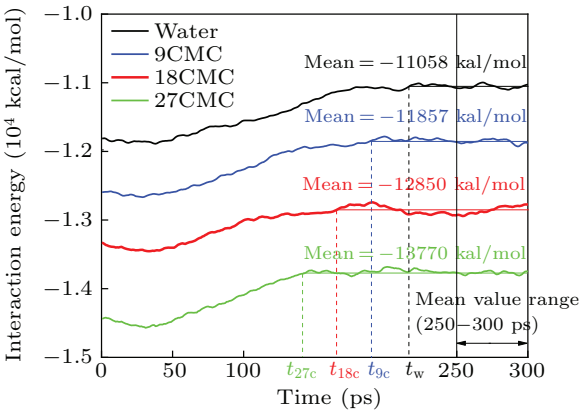


Fig. 6. Variation of interaction energy with time.

3.3. Molecule number density distribution

After optimizing the simulation systems in Fig. 7(a), the distribution of the solution molecules perpendicular to the direction of the flow changes. As shown in Fig. 7(b), some of

the solution molecules tend to distribute towards the walls. The molecule number density near the walls increases significantly. This was also reported in an MD simulation of Ar atoms[34] and hexadecane fluid.[35] As shown in Fig. 7(c), two layers (layer 1 and layer 2) with a higher molecule number density were formed near the walls. Layer 1 has a higher number density, as seen from the conformation diagram (Fig. 7(c)).

The number density profile of the solution layer was calculated and is shown in Fig. 7(d). There are two peaks near the walls and the number density of layer 1 is much higher than that of layer 2. The calculation results confirmed the formation of two layers with a larger number of particles when the solution is in the microchannel.

In order to explain the reason behind the velocity profile variation in Fig. 3, the number density of the particles in the solution layer was calculated under different conditions. Figure 8(a) shows the average number density of the four solutions in 200 ps.

It can be seen that peaks of number density exist in layer 1 ($P_{w1} > P_{9c1} > P_{18c1} > P_{27c1}$) and layer 2 ($P_{w2} > P_{9c2} > P_{18c2} > P_{27c2}$) in all four solutions, which means that the non-Newtonian and Newtonian fluids have the same particle distribution when they flow in the same microchannel. Water has the largest peak in layer 1 (P_{w1}) and layer 2 (P_{w2}), followed by 9CMC (P_{9c1}, P_{9c2}), 18CMC (P_{18c1}, P_{18c2}) and 27CMC (P_{27c1}, P_{27c2}). This indicates that CMC molecules have an attractive effect on the water molecules in the CMC solutions and tend to attract water molecules around them, reducing the number of water molecules near the walls. Higher concentrations of CMC solutions, such as 27CMC, which have more CMC molecules, are more attractive to water, resulting in lower peaks near the walls.

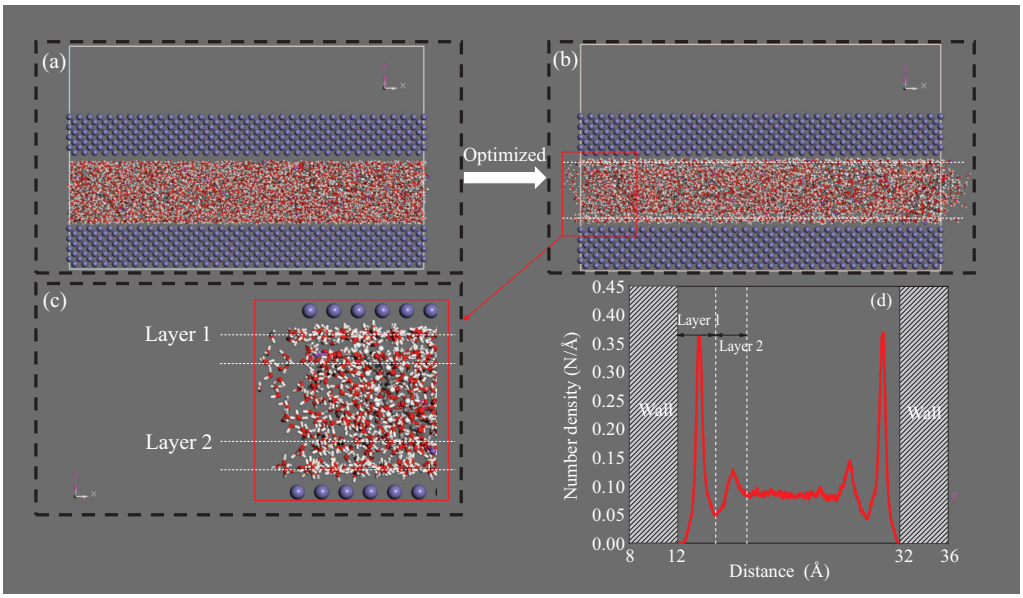


Fig. 7. (a) The simulation system before optimization. (b) The optimized simulation system. (c) The layered solution. (d) The variation of number density with distance.

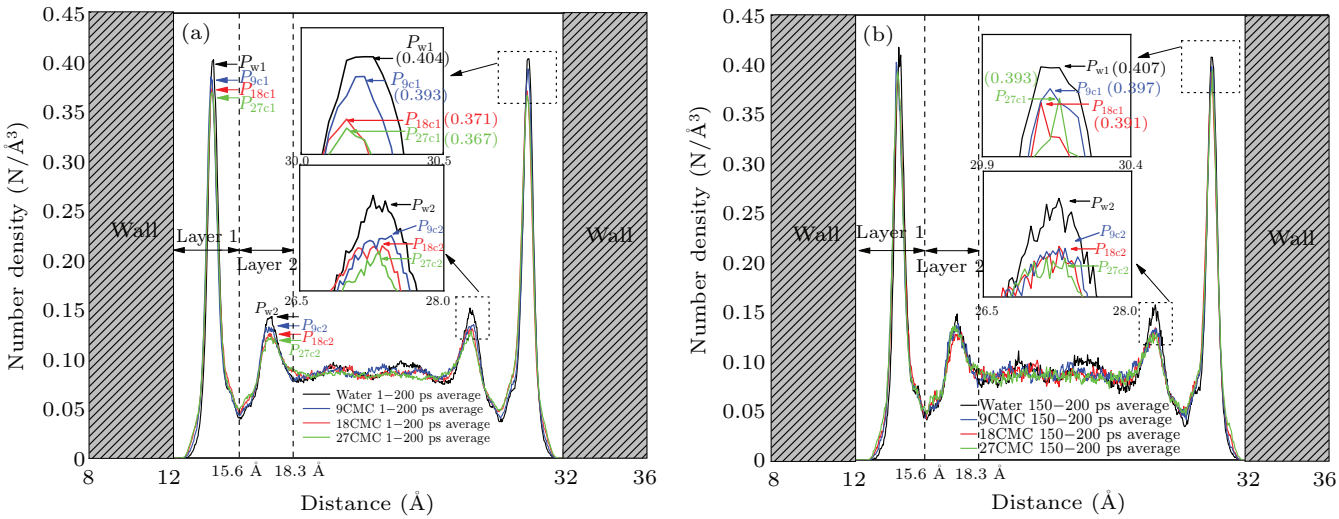


Fig. 8. (a) The number density of CMC and water solution layers (1–200 ps). (b) The number density of CMC and water solution layers (150–200 ps).

The values of the velocity profile of a fluid are inversely related to the molecule number density at that position. It can be seen from Fig. 8(a) that water has the largest number density in layer 1 and layer 2, but it does have the smallest velocity in Fig. 3. Similarly, the CMC solution with the highest concentration has the largest velocity profile values in layer 1 and layer 2. However, it has the smallest number density in Fig. 8(a). This shows that the molecule number density and velocity are inversely proportional. The greater the number density, the greater the flow resistance at that position, and it is more difficult to obtain a larger velocity profile value.

Figure 8(b) shows the average number density at a higher velocity (150–200 ps). It is shown that, at higher velocity, the value of P_{c1} is larger than the result in Fig. 8(a), while the P_{w1} has almost no change. P_{c1} increased more for higher concentration solutions. At a higher velocity, the CMC solution is subject to a stronger shearing effect and more particles are distributed at the boundaries. The P_{w1} of water hardly changes significantly with velocity because water has no shear-thinning properties.

In order to obtain the effect of velocity on the number density, two acceleration intervals (1–50 ps and 150–200 ps) were selected to represent different flow velocities and the number density of four solutions at two different velocities was calculated, as shown in Fig. 9.

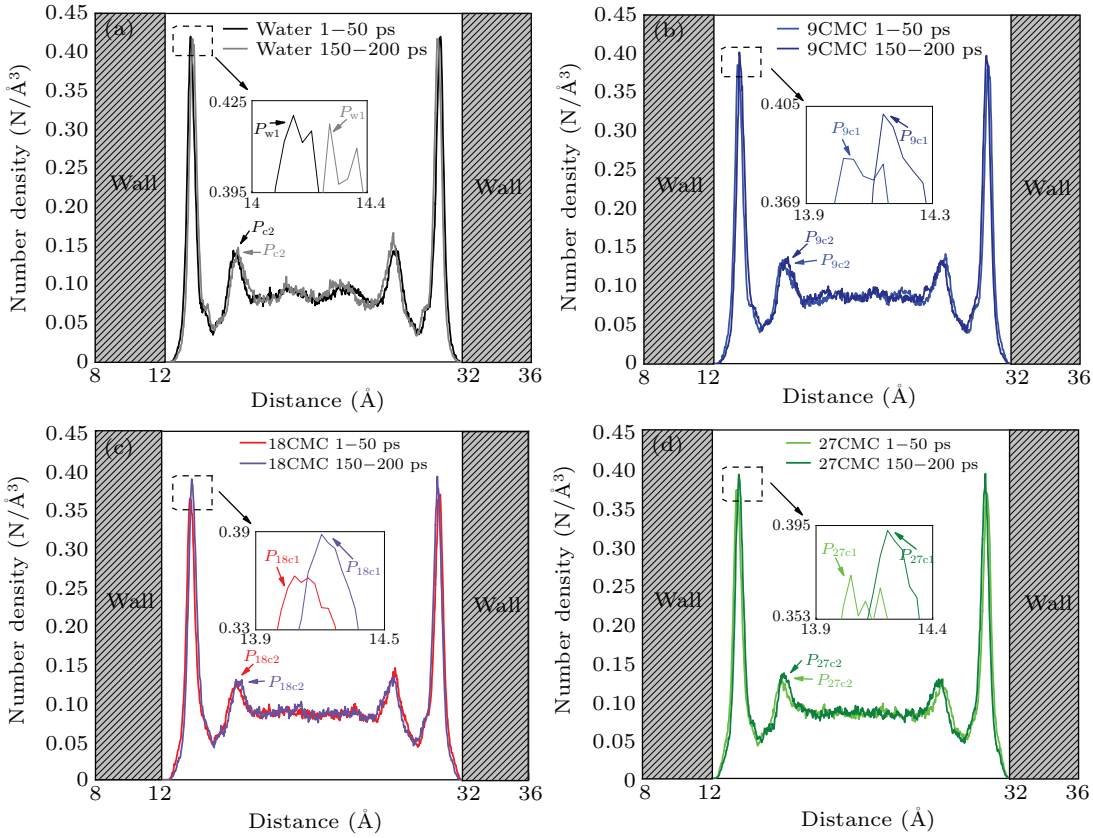


Fig. 9. (a) The number density of water under different velocities. (b) The number density of 9CMC under different velocities. (c) The number density of 18CMC under different velocities. (d) The number density of 27CMC under different velocities.

It is shown in Fig. 9(a) that, as the velocity increases, the distribution of particles in water is almost constant (P_{w1} remains constant), so the particle distribution of Newtonian fluid is not affected by the flow velocity. As shown in Figs. 9(b)–9(d), different from water, the particle distribution of shear-thinning fluid changes with the flow velocity increase. The P_{c1} increases as the velocity increases for CMC solutions and the peak value increases by about 9%. This shows that when the flow velocity of non-Newtonian fluid in the microchannel increases, the particle distribution of its internal molecules changes. As the velocity increases, the molecule number density near the walls increases.

3.4. Hydrogen bonding in the solution

The RDF of the hydrogen atoms on the CMC molecules (H_c) and the oxygen atoms on the water molecules (O_w) was calculated to determine their interaction (H-bond).

The RDF is the calculation of the relative probability of finding particle B at distance r from the reference particle A

$$g(r) = \frac{\mathrm{d}N}{4\rho\pi^2 r^2 \mathrm{d}r}, \tag{7}$$

where $\mathrm{d}N$ is the number of molecules between r and $r + \mathrm{d}r$ from atom A, and ρ is the average density of atom B.

The solution layer is in a state of accelerating motion. The average RDF was calculated between H_c and O_w at 1–50 ps

and 150–200 ps to obtain two flow states with different velocities.

As shown in Figs. 10(b)–10(d), there is a peak value when the distance between H_c and O_w is 2–3.5 Å, which is in the range of hydrogen bonding.[36] The peak value decreases as the velocity increases. This indicates that the hydrogen bonding between H_c and O_w weakens as the shear rate increases. The viscosity of a solution comes from the mutual attraction between molecules. After CMC molecules are added to water, they interact with water molecules, increasing the attraction between molecules in the solution and increasing the solution's viscosity, which is higher than the original water viscosity. Our previous work found that the weakening of hydrogen bonding between water and CMC molecules leads to decreased solution viscosity when shear is applied to shear-thinning fluids. That is because the attraction between CMC and water molecules is weakened by shearing and this is more conducive to the movement of the CMC molecules, causing the solution viscosity to decrease.[18] Since the flow we analyzed in the previous study was Couette flow, its shearing effect on the solution was stronger, resulting in more H_c–O_w reduction, and the peak values were reduced even more. The Poiseuille flow studied in this paper has a slightly weaker shearing effect on the solution and its peak values drop less.

According to the result of RDF, water molecules begin to move away from CMC molecules as the shear rate increases due to the weakening of hydrogen bonding. Combining the conclusions drawn in Subsection 3.3, it can be inferred that the water molecules tend to break away from the bonds of CMC molecules and distribute towards the walls, as shown in the stress state diagram of molecules in the solutions (Fig. 10(a)). In conclusion, with the increase of the flow velocity, the hydrogen bonding of H_c–O_w weakens so that the molecule number density distribution in the CMC solution changes and the viscosity of the solution decreases, leading to the shear-thinning characteristics of non-Newtonian fluid.

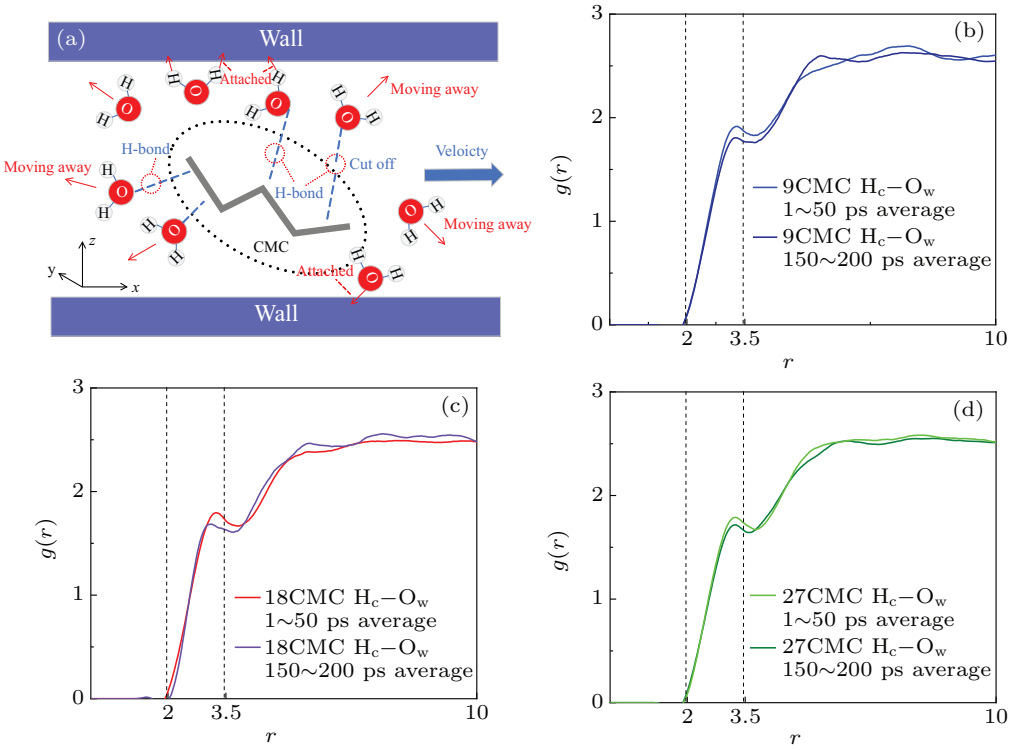


Fig. 10. (a) Stress state diagram of molecules in the solution when flowing. (b) RDF of H_c–O_w in 9CMC. (c) RDF of H_c–O_w in 18CMC. (d) RDF of H_c–O_w in 27CMC.

4. Conclusion

In this study, the flow mechanism of non-Newtonian fluids in a microchannel was simulated by MD. The flow was simulated using an acceleration field to drive the fluid between two walls. By analyzing the molecular coordinate information of the simulation system, the following conclusions are obtained.

(1) The velocity profile shape and the interaction energy between the walls and the fluid can reflect the non-Newtonian characteristics. The top-hat shape intensifies as the power law index of the fluid decreases. The interaction energy gradually decreases and reaches a steady state as the fluid flows. The non-Newtonian fluid's energy falls faster because of a decrease in its viscosity.

(2) The molecule number density of the fluid near the walls is higher, forming two peaks of number density near the walls. Because of the attraction of CMC molecules to water, the peak values with higher concentrations are lower. With the

increase in velocity, the peak of the CMC solution increases, and the value is inversely proportional to the velocity profile.

(3) The fluid is sheared as it flows and, with an increase of the fluid velocity, the H_c–O_w hydrogen bonding weakens, resulting in a decrease in solution viscosity. Due to the shear-thinning effect, the water molecules break away from the CMC molecules and tend to distribute toward the wall.

Acknowledgement

Project supported by the National Natural Science Foundation of China (Grant Nos. 51775077 and 51909023).

References

[1] Nair R and Choudhury A R 2020 *Int. J. Biol. Macromol.* **159** 922
[2] Yang Z C, Bi Q C, Liu B and Huang K X 2010 *Int. J. Multiph. Flow* **36** 60
[3] Laporte M, Montillet A, Belkadi A, Valle D D, Loisel C, Riaublanc A and Hauser J L 2020 *Chem. Eng. Process.* **148** 107787
[4] Megahed A M 2013 *Chin. Phys. B* **22** 974701
[5] Nazir S and Kwon O S 2022 *Appl. Sci. Converg. Technol.* **31** 40
[6] Economidou S N, Uddin M J, Marques M J, Douroumis D, Sow W T, Li H, Reid A, Windmill J F C and Podoleanu A 2021 *Addit. Manuf.* **38** 101815
[7] Luo T, Fan L, Zhu R and Sun D 2019 *Micromachines* **10** 104
[8] Lee C Y, Chang C L, Wang Y N and Fu L M 2011 *Int. J. Mol. Sci.* **12** 3263
[9] Kawahara A, Yonemoto Y and Arakaki Y 2020 *Flow Turbul. Combust.* **105** 1325
[10] Mansour M H, Kawahara A and Sadatomi M 2015 *Int. J. Multiph. Flow* **72** 263
[11] Ansari S, Rashid M A I, Waghmare P R and Nobes D S 2020 *SN Appl. Sci.* **2** 1787
[12] Miansari M, Aghajani H, Zarringhalam M and Toghraie D 2020 *J. Therm. Anal. Calorim.* **144** 179
[13] Wu W W, Sun S L, Wang Z Z and Ding S 2019 *Mech. Mater.* **139** 103187
[14] Lemarchand C A, Bailey N P, Todd B D, Daivis P J and Hansen J S 2015 *J. Chem. Phys.* **142** 244501
[15] Chen K H, Wang Y, Xuan S H and Gong X L 2017 *J. Colloid Interface Sci.* **497** 378
[16] Bidault X, Chaussedent S, Blanc W and Neuville D R 2016 *J. Non-Cryst. Solids* **433** 38
[17] Blanco-Díaz E G, Castrejón-González E O, Alvarado J F J, Estrada-Baltazar A and Castillo-Borja F 2017 *J. Mol. Liq.* **242** 265
[18] Yang G, Zheng T, Cheng Q H and Zhang H C 2021 *Acta Phys. Sin.* **70** 124701 (in Chinese)
[19] Wang B, Cavallo D and Chen J B 2020 *Polym. J.* **210** 123000
[20] Castillo-Tejas J, Castrejón-González O, Carro S, González-Coronel V, Alvarado J F J and Manero O 2016 *Colloids Surf. A-Physicochem. Eng. Asp.* **491** 37
[21] Sun H J 1998 *J. Phys. Chem. B* **102** 7338
[22] Ewald P P 1921 *Ann. Phys.* **369** 253
[23] Cao B Y, Chen M and Guo Z Y 2006 *Phys. Rev. E* **74** 066311
[24] Abiev R S 2022 *Chem. Eng. Sci.* **250** 117380
[25] Yang G, Feng K and Zhang H C 2023 *Chem. Eng. Res. Des.* **197** 405
[26] Lewis J M and Wang Y 2019 *Int. J. Heat Mass Transf.* **128** 649
[27] Cao Z, Wu Z and Sundén B 2018 *Chem. Eng. J.* **344** 604
[28] Mondal S and Majumder S K 2018 *Exp. Therm. Fluid Sci.* **94** 215
[29] Alipour P, Toghraie D, Karimipour A and Hajian M 2019 *J. Mol. Liq.* **275** 192
[30] Faraji F, Rajabpour A and Kowsary F 2016 *J. Mech. Sci. Technol.* **30** 803
[31] Feng K and Zhang H C 2021 *Chem. Eng. Res. Des.* **173** 158
[32] Abiev R S 2022 *Chem. Eng. Sci.* **247** 116930
[33] Zhang Z Q, Zhang H W and Ye H F 2009 *Appl. Phys. Lett.* **95** 154101
[34] Semiromi D T and Azimian A R 2010 *Heat Mass Transf.* **46** 791
[35] Li J, Zhu P, Sheng Y Y, Liu L and Luo Y 2021 *Chin. Phys. B* **30** 080205
[36] Kumar R, Schmidt J R and Skinner J L 2007 *J. Chem. Phys.* **126** 204107